



Lower Ionospheric variation over Europe during the tectonic activity in the area of Thessaly, Greece, on March of 2021.

Michael E. Contadakis¹, Demeter N. Arabelos¹, Christos Pikridas¹, Stylianos Bitharis¹, and Emmanuel Scordilis²

¹ Department of Surveying & Geodesy University of Thessaloniki, Greece

² Department of Geophysics, Aristotle University of Thessaloniki, Greece

Abstract: This is one of a series of papers in which we investigate the Lower ionospheric variation on the occasion of intense tectonic activity. In the present paper, we investigate the TEC variations during the intense seismic activity in Thessaly, on March 2021 over Europe. The Total Electron Content (TEC) data are been provided by the Hermes GNSS Network managed by GNSS_QC, AUTH Greece, the HxGN/SmartNet-Greece of Metrica S.A, and the EUREF Network. These data were analysed using Discrete Fourier Analysis in order to investigate the TEC turbulence. The results of this investigation indicate that the High-Frequency limit, f_o , of the ionospheric turbulence content, increases as approaching the occurrence time of the earthquake, pointing to the earthquake epicenter, in accordance to our previous investigations. We conclude that the Lithosphere Atmosphere Ionosphere Coupling, LAIC, mechanism through acoustic or gravity waves could explain this phenomenology.

Keywords: Seismicity, Lower Ionosphere, Ionospheric Turbulence, Brownian Walk, Aegean area.

1. Introduction

It is argued that tectonic activity during the earthquake preparation period produces anomalies at the ground level, which propagate upwards in the troposphere as Acoustic or Standing gravity waves (Miyaki et al. 2002; Hayakawa et al. 2011; Hayakawa 2011; Hayakawa et al. 2018). These Acoustic or Gravity waves affect the turbidity of the lower ionosphere, where sporadic Es-layers may appear too, and the turbidity of the F layer. Subsequently the produced disturbance starts to propagate in the ionosphere's waveguide as gravity wave. The inherent frequencies of the acoustic or gravity wave range between 0.003Hz (period \approx 5min) and 0.0002Hz (period \approx 100min), which, according to Molchanov et al. (2004, 2006), correspond to the frequencies of the turbulent produced by tectonic activity during the earthquake preparation period. During this propagation, the higher frequencies are progressively dumped. Thus, observing the frequency content of the ionospheric turbidity, we will observe a decrease of the higher limit of the turbidity frequency band as we move away from the locus of the disturbance. This paper is one of a series of similar papers in which we investigate the Lower ionospheric variations from TEC observations during an intense seismic activity. In the present paper, we investigate the TEC variations over Europe during the intense seismic activity in Thessaly (Greece), on March 2021. The Total Electron Content (TEC) data are been provided by the Hermes GNSS

Network managed by GNSS_QC, AUTH Greece, the HxGN/SmartNet-Greece of Metrica S.A, and the EUREF Network. These data were analysed using Discrete Fourier Analysis in order to investigate the TEC turbulence.

2. The Tirnavos Mainshock M6.3, Central Greece, March 3, 2021

On March 3, 2021 (10:16 UTC, 12:16 local time), a strong earthquake of magnitude M6.3 occurred close to the city of Larissa (central Greece), ~8km to the west of the city of Tirnavos. (Chatzipetros et al. 2021; Karakostas et al. 2021).

The area where the seismic sequence occurred is characterized by moderate seismicity with most of the strong earthquakes of the past having occurred in the wider vicinity of the mainshock's epicenter. Table 1 lists the focal parameters of the most important ($M \geq 6.0$) earthquakes that occurred since the 16th century in the broader region (figure 1). It is observed that their magnitudes have values very close to the magnitude of the mainshock under study, implying that the M6.3 mainshock can be considered as a characteristic earthquake of this region.

Table 1. Focal parameters of the strong ($M \geq 6.0$) earthquakes that occurred in the broader region of the sequence under study, since the 16th century.

Year	Date	Lat(°N)	Lon(°E)	M
1544	April 24	39.50	21.60	6.4
1621	March 06	39.50	21.90	6.0
1661	March 30	39.50	22.10	6.2
1665	October 30	39.60	21.60	6.0
1668	August	39.70	22.40	6.0
1731	-	39.70	22.50	6.0
1766	November 09	39.80	22.30	6.1
1781	September 08	39.60	22.40	6.2
1905	January 20	39.70	22.90	6.4
1941	March 01	39.70	22.50	6.3

The broader region is dominated by nearly WNW-ESE striking faults, connected to an almost N-S extensional stress field (Papazachos and Papazachou 2003). The fault plane solutions of the strongest earthquakes of the present sequence, issued by reliable sources (e.g. GCMT, USGS, NOA, AUTH, INGV, KOERI, GFZ, ERD), are relative to each other. They are all showing that the seismic fault is striking at an azimuth of ~320° and dipping to the NE at an angle of ~40° (<https://www.emsc-csem.org/Earthquake/tensors.php>) with a rake angle of nearly -80° (normal faulting with a negligible left lateral component).

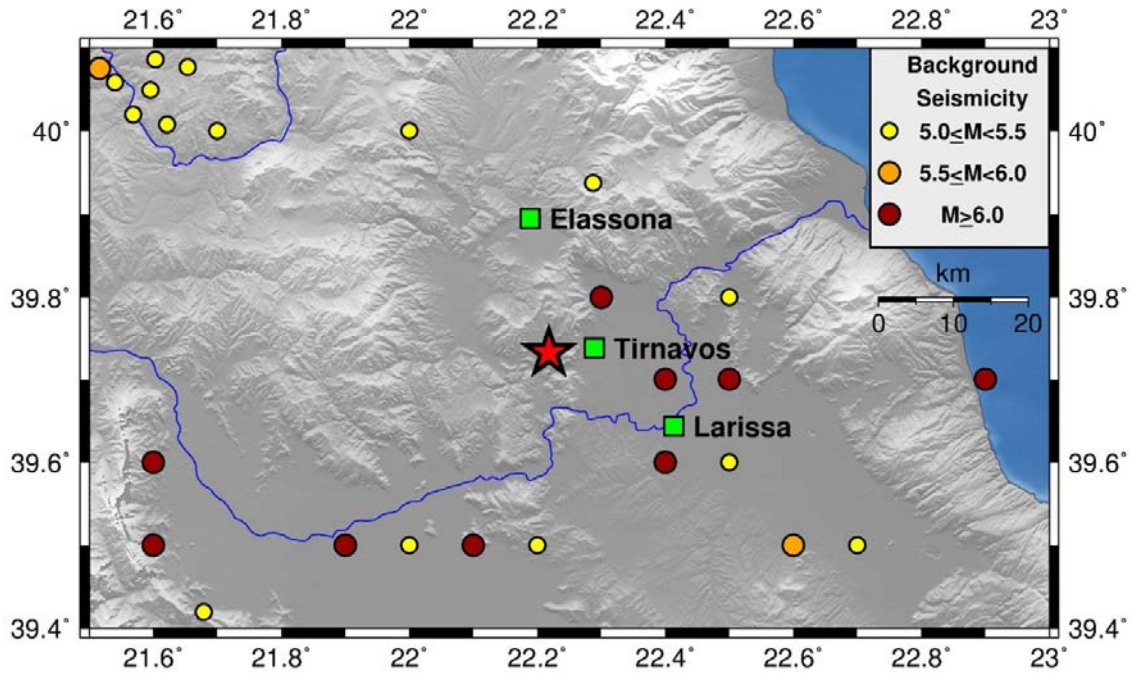


Figure 1. Epicenters (coloured circles) corresponding to the background seismicity (since 1500) of the broader region of the recent Tirnavos earthquake (red star). Green squares denote the three larger cities (Larissa, Tirnavos and Ellassona), close to the epicentral area.

The M6.3 main shock was followed by a rather intensive (regarding the frequency and magnitudes) aftershock sequence (table 2). Its strongest aftershock with M6.0 took place the next day after the main shock, expanding the excited area to the NW. The spatial distribution of the epicenters of the sequence is given in figure 2. The focal parameters of the earthquakes-members of the sequence are coming from the online catalogues of the Department of Geophysics of the Aristotle University of Thessaloniki (<http://geophysics.geo.auth.gr/ss/CATALOGS/preliminary/prelcatDB.txt>) and of the Geodynamic Institute of the National Observatory of Athens (<http://bbnet.gein.noa.gr/HL/database>).

Table 2. Focal parameters of the strongest ($M \geq 5.0$) earthquakes of the aftershock sequence of the present study.

Date	Time (UTC)	Lat (°N)	Lon (°E)	M
March 03, 2021	10:16:08	39.7322	22.2180	6.3
March 03, 2021	18:24:08	39.7208	22.0803	5.1
March 04, 2021	18:38:17	39.7818	22.1165	6.0
March 04, 2021	19:23:51	39.8054	21.9221	5.1
March 12, 2021	12:57:50	39.8130	21.9870	5.6

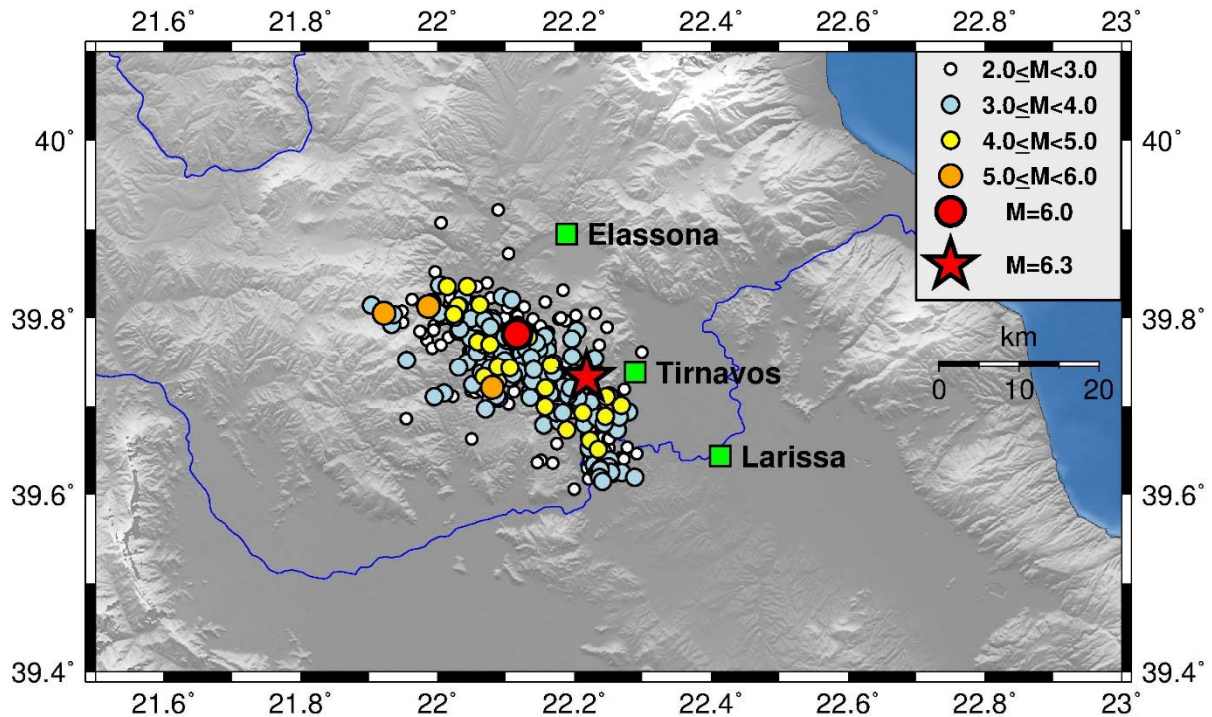


Figure 2. Spatial distribution of the aftershocks of the M6.3 main shock. Different dimensions/colors of the symbols correspond to different magnitude classes. The red star denotes the epicenter of the mainshock while the red circle is the epicenter of the strongest aftershock (March 4, M6.0).

3. TEC Variation Over Mid Latitudes of Europe

TEC values from each dual frequency GPS receiver records (especially, the GPS-TEC software) and the TEC values of several GNSS permanent stations were estimated before and after the occurrence of the earthquakes under study. The stations record satellite data with a 30-sec observation rate. Most of the stations participate to EPN/EUREF network while some of them belong to local permanent networks of Greece such as Hermes Net and HxGN/Smart Net-Greece. The selected stations are located nearby the geographic latitudes of the epicentres of the seismic sequence. The TEC values were estimated using the IONosphere Map Exchange (IONEX) Format (Schaer et al. 1998) files, where the hourly TEC values from a large network of ten GPS/GNSS stations all over Europe for the test period were estimated (Pikridas et al. 2019). The processing scenario was applied using the IONEX files that are available at the Center for Orbit Determination (CODE). The TEC parameter is modelled by a spherical harmonic expansion up to 15 degrees and order 15 referring to a solar-geomagnetic reference frame. The produced ionospheric product is regarded as one with the most precise TEC information. As it concerns, the TEC estimation for each PRN of the observed satellites included in the selected permanent stations RINEX data, the GPS-TEC software (Seemala and Valladares 2011) was used considering the receiver and inter-channel biases for different satellites in the receiver. The GPS-TEC software was used to derive the phase and code value L1 and L2 GPS frequencies to eliminate the effect of clock errors and tropospheric water vapour to calculate relative values of slant or line-of-sight TEC. TEC

values for each observed satellite such as PRN1 (which is studied in detail) are derived with time resolution of one (1) minute. A single-layer approximation is adopted to convert slant TEC (STEC) into vertical (VTEC) values, where ionospheric pierce point is considered at an altitude of 350 km above the earth's surface. For the purposes of our investigation, we analyze the variations of TEC over the broader area of Mediterranean before and during the seismic activity of the last quarter of 2021 in the area of Thessaly, on March 2021 ($\varphi=39.7322^{\circ}\text{N}$, $\lambda=22.2180^{\circ}\text{E}$). Thus, we use the TEC estimations from EUREF stations of distances ranging from 0 km to 2824.2km from active areas, for the period 01/09/2021-03/03/2021. The selected GPS stations have about the same latitude and are expected to be affected equally from the Equatorial Anomaly as well as from the Auroral storms. Table 3 displays the coordinates and the epicentral distances of the GPS stations while Figure 3 displays their locations as well as the epicenter of the strongest event. Figure 4 displays, as an example, the TEC variation over three GPS stations during March of 2021.

Table 3. *Coordinates and epicentral distances of the GPS stations.*

GPS Station	Latitude ($^{\circ}\text{N}$)	Longitude ($^{\circ}\text{E}$)	Epic.Dist. (km)
Istanbul	41.016791	28.979870	744.6
Thessaloniki	40.641282	22.944230	73.4
Tirnavos	39.764222	22.284092	0
Ohrid	41.123657	20.801771	164.8
USAL	40.335000	18.111000	464.1
Mate	40.667598	16.604398	631.6
Toulouse	43.606979	1.4442091	2317.6
Yebe	40.533649	-3.111166	2824.2

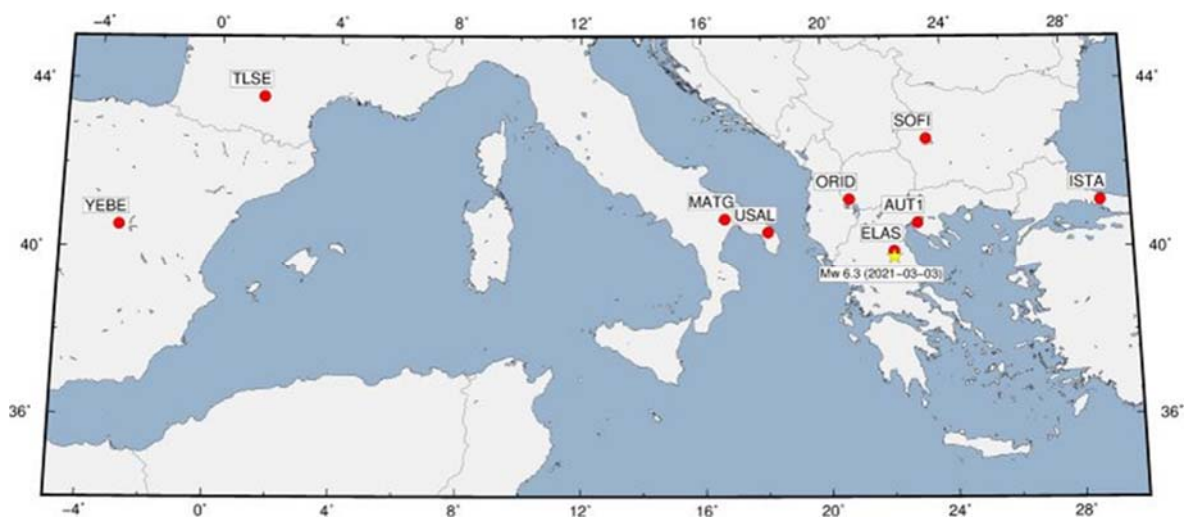


Figure 3. *The GPS stations (red circles) and the epicenter (yellow star) of the main shock of Tirnavos earthquake.*

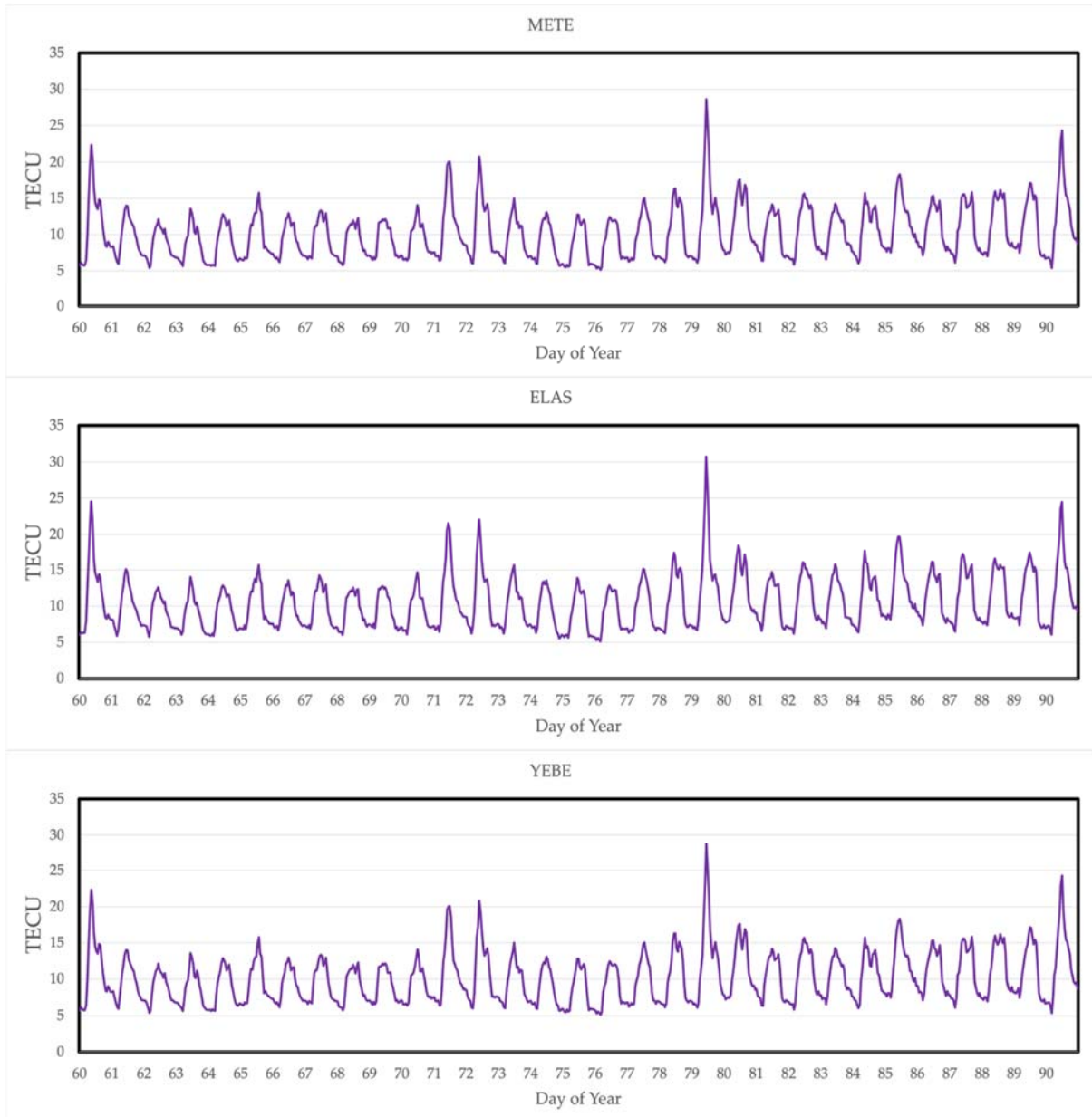


Figure 4. TEC variation over the selected GPS stations during March of 2021

4. Geomagnetic and Solar Activity Indices

The variations of the geomagnetic field were followed by the Dst- index and the planetary kp three-hour indices quoted from the site of the Space Magnetism Faculty of Science, Kyoto University (<https://wdc.kugi.kyoto-u.ac.jp/index.html>) for the time period of our data. Figure 5 presents the Dst-index variation during March of 2021.

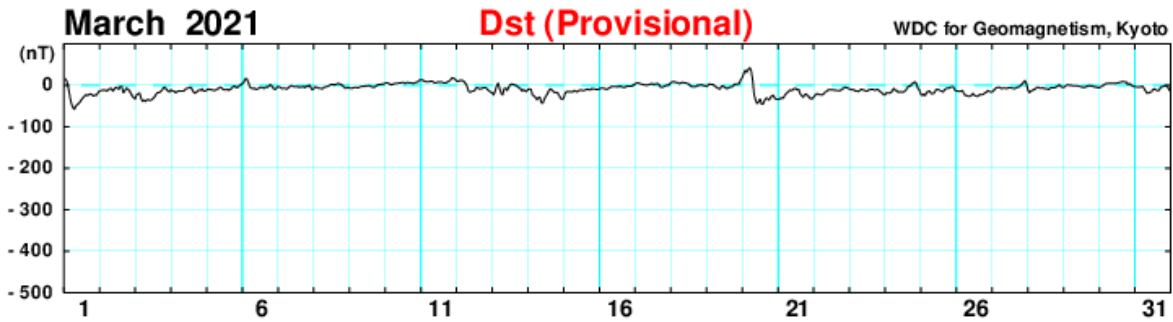


Figure 5. *Dst-index variation during March of 2021*

5. Data Process

The Power Spectrum of TEC variations will provide information on the frequency content of them. Apart of the well-known and well-expressed tidal variations, for which the reliability of their identification can be easily inferred by statistical tests, small amplitude space-temporal transient variations cannot have any reliable identification by means of a statistical test. Nevertheless looking at the logarithmic power spectrum, we can recognize from the slope of the diagram whether the contributed variations to the spectrum are random or periodical. If they are random the slope will be 0, which corresponds to the white noise, or -2 which corresponds to the Brownian walk noise, otherwise the slope will be different, the so called Fractal Brownian walk (Turcotte 1997). This means that we can trace the presence of periodical variations in the logarithmic power spectrum of TEC variations. As an example, Figure 6 displays the logarithmic power spectrum of TEC variations over the GPS station of Thessaloniki (Greece) on 03/03/2021. It is seen that the slope of the diagram up to $\log(f_o)=-3.78$ is $b=-2$ (Brownian walk noise) and for $\log(f_o)<-3.3$ is $b=-1$ (fractal Brownian walk noise). This means that for frequencies higher than $f_o=\exp(-3.3)=0.0228=760.75\mu\text{Hz}$ the TEC variation is random noise. On the contrary, the TEC for lower frequencies exhibits not random variations, i.e. turbulent. So we conclude that the upper limit of the turbulent band is $f_o=\exp(-3.78)=0.0228\text{cycl}/0.5\text{min}\Rightarrow 760.75\mu\text{Hz}$ Equivalently, the lower period limit P_o of the contained turbulent is 21.908 minutes.

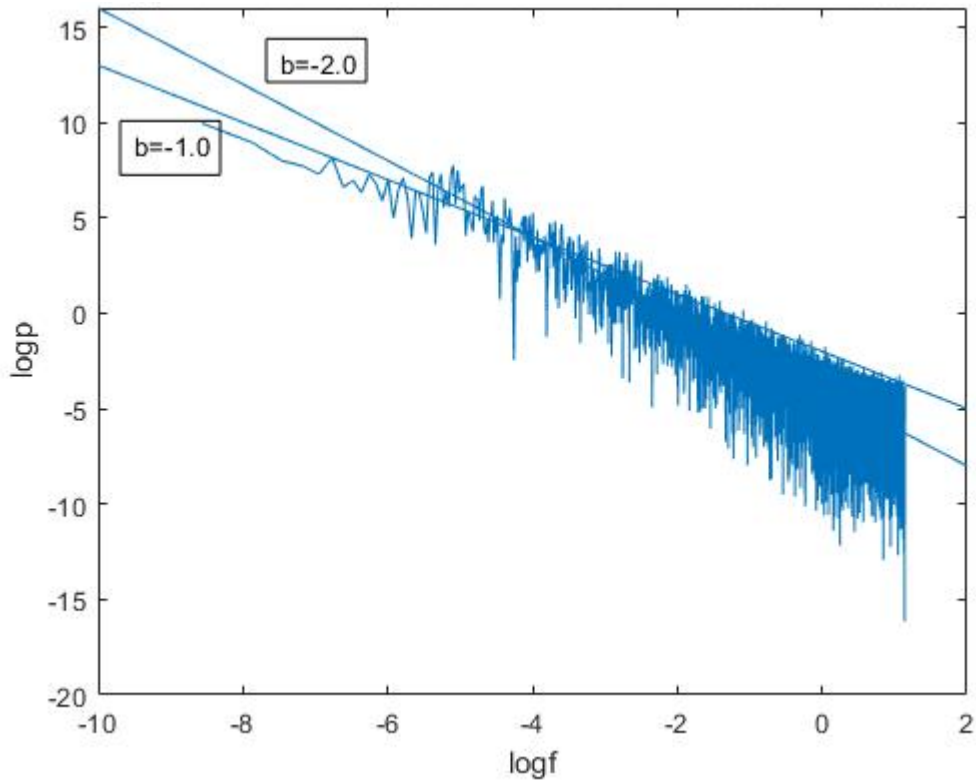


Figure 6. *Logarithmic power spectrum of TEC variations over Thessaloniki (Greece) on October 3, 2021.*

6. Results

Figures 7 and 8 display the variation of the TEC turbulence frequency band upper limit f_o with time and epicentral distance from the Tirnavos main shock of 03/03/2021, while Figures 9 and 10 display the respective variation of the period lower limit P_o . It is shown that a strong dependence of the upper frequency f_o limit (lower period limit P_o) of the ionospheric turbulent band content with time and with epicentral distances is observed. In particular, the closer in time of the main shock or in space to the active area the higher frequency f_o limit (lower period P_o), is. The observed frequencies (and the respective periods) are in the range of the observed Acoustic Gravity Waves on the occasions of strong earthquakes, which correspond to periods of 30 to 100min (Molchanov et al. 2004; Molchanov et al. 2005) or 20 to 80min (Horie et al. 2007).

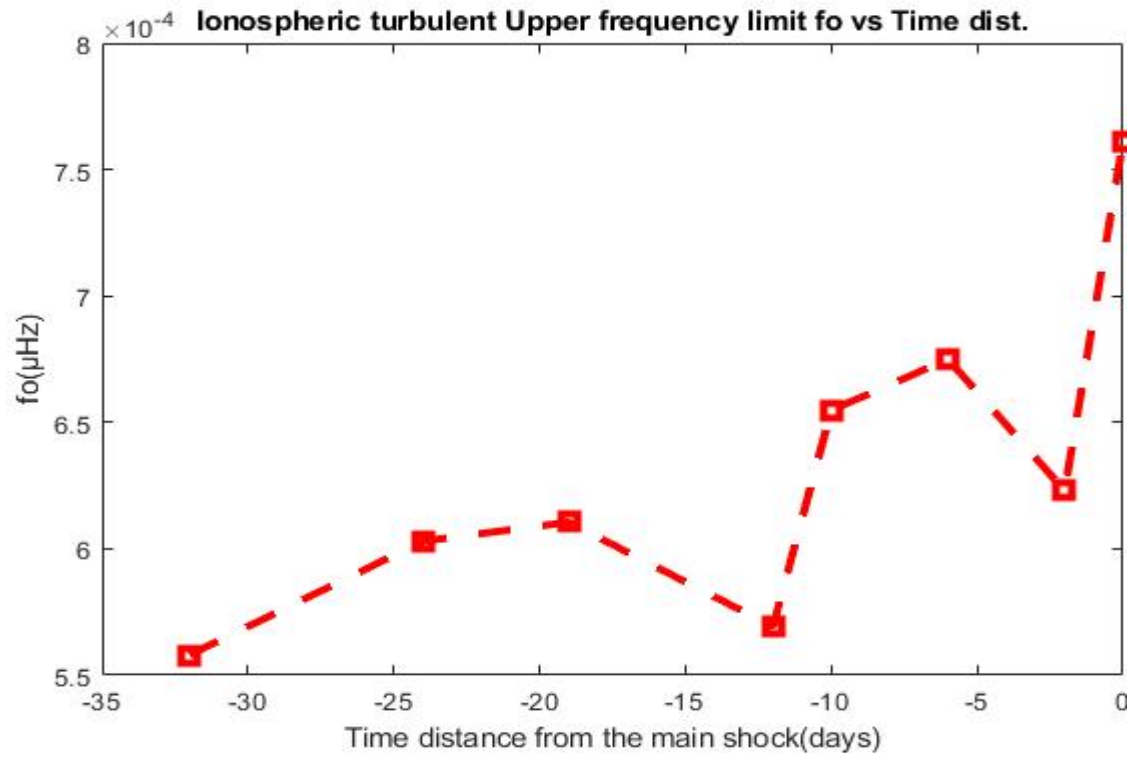


Figure 7. TEC turbulence band upper limit f_o versus time to the Tirnavos main shock.

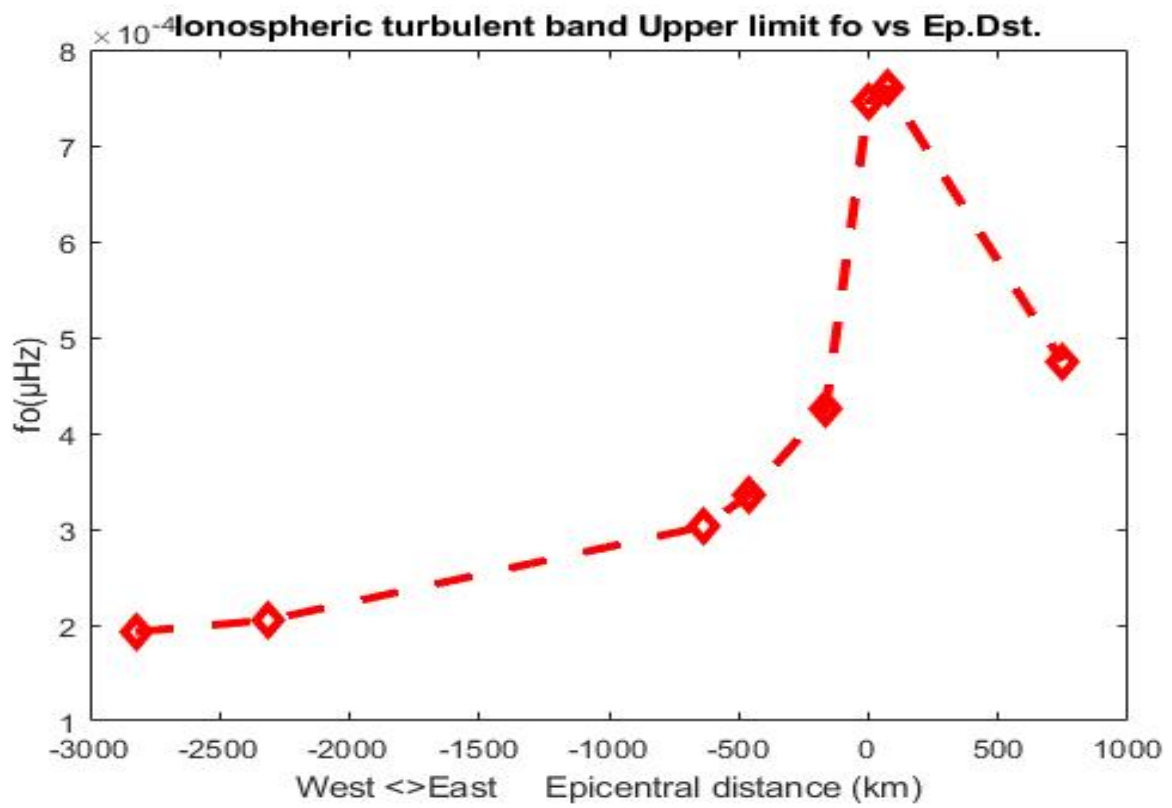


Figure 8. TEC turbulence band upper limit f_o versus epicentral distance from Tirnavos main shock.

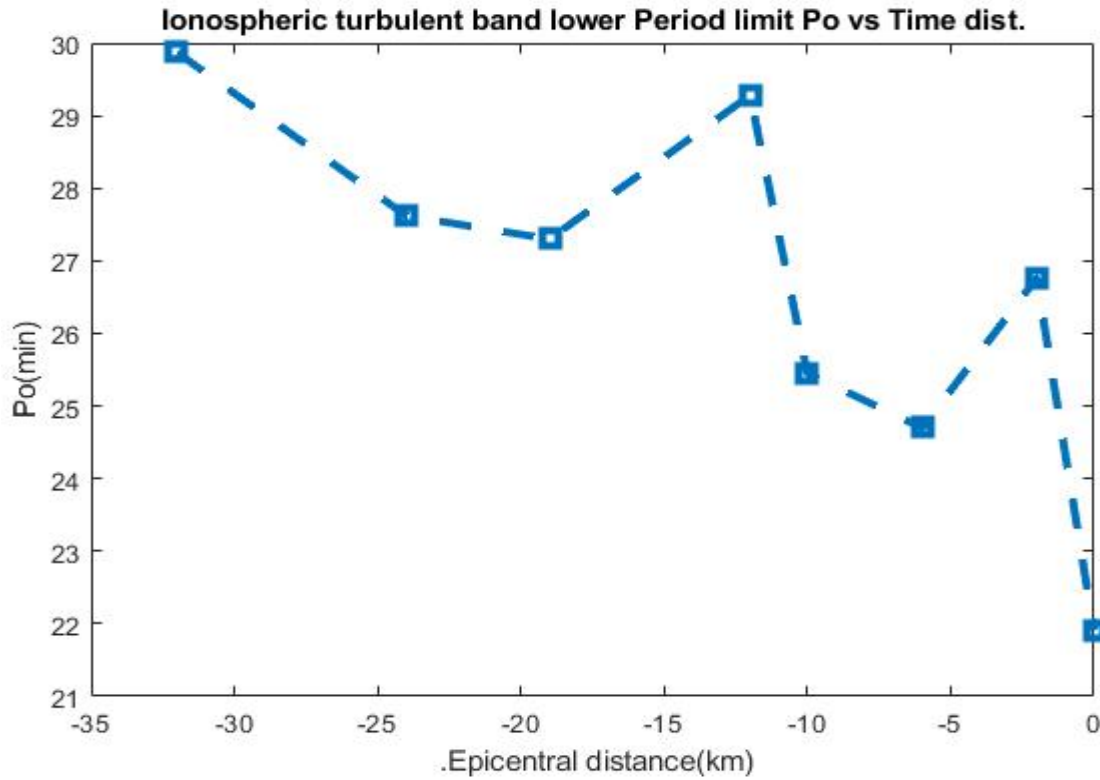


Figure 9. TEC turbulence band lower period limit P_o versus time to the Tirnavos main shock.

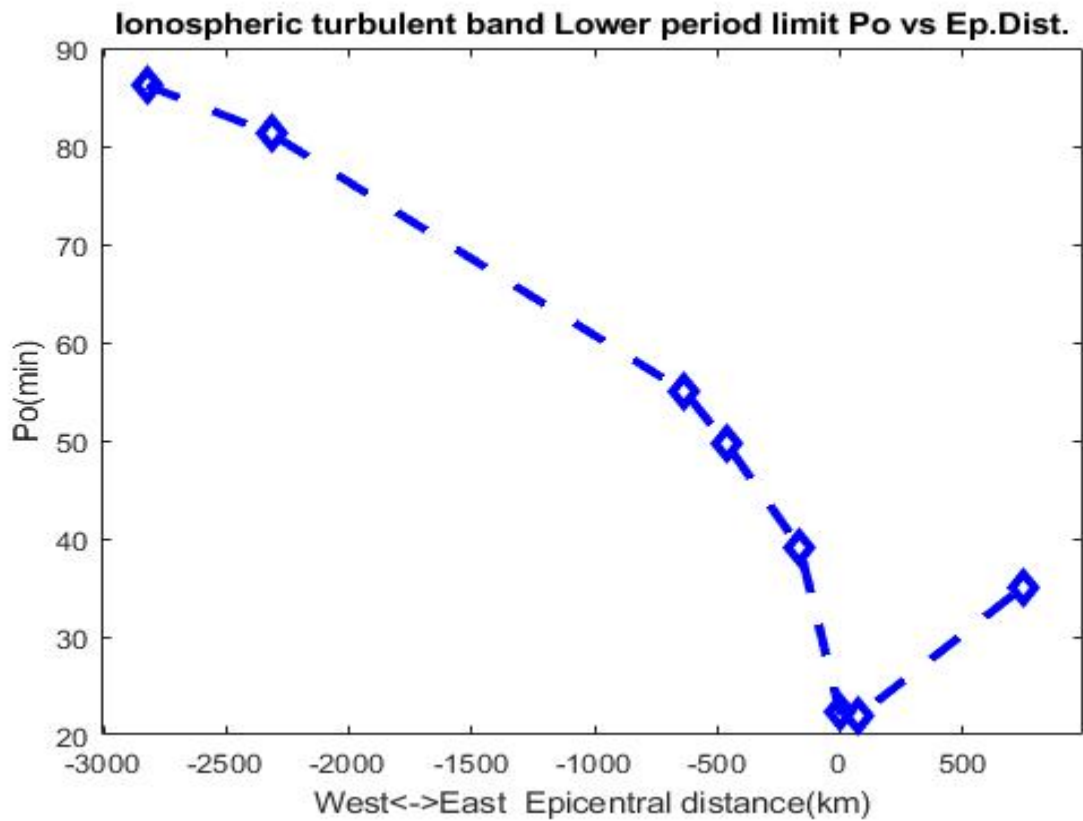


Figure 10. TEC turbulence band lower period limit P_o versus epicentral distance from Tirnavos main shock.

Hobara et al. (2005) in a study on the ionospheric turbulence in low latitudes concluded that the attribution of the turbulence to earthquake process and not to other sources, i.e. solar activity, storms etc., is not conclusive. Nevertheless in our case, the steady monotonic, time and space, convergence of the frequency band upper limit f_o increment, to the occurrence of the examined strong earthquakes is a strong indication that the observed turbulence is generated by the respective earthquake preparation process. The qualitative explanation of this phenomenology can be offered on the basis of the Lithosphere Atmosphere Ionosphere Coupling, LAIC: Tectonic activity during the earthquake preparation period produces anomalies at the ground level which propagate upwards in the troposphere as acoustic or standing gravity waves (Hayakawa et al. 2011; Hayakawa 2011). These acoustic or gravity waves affect both, the turbulence of the lower ionosphere, where sporadic Es-layers may appear too (Liperovsky et al. 2005), and the turbulence of the F-layer. Subsequently, the produced disturbance starts to propagate in the ionosphere's waveguide as gravity wave and the inherent frequencies of the acoustic or gravity waves can be traced on TEC variations [i.e. the frequencies between 0.003Hz (period 5min) and 0.0002Hz (period 100min)]. These frequencies, according to Molchanov et al. (2004, 2005) and Horie et al. (2007), correspond to the frequencies of the turbulent induced by the LAIC coupling process to the ionosphere. As we move far from the disturbed point, in time or in space, the higher frequencies (shorter wavelength) variations are progressively attenuated.

7. Conclusions

The results of this investigation indicate that the High-Frequency limit f_o of the ionospheric turbulence content, increases as approaching the occurrence time of the earthquake, pointing to the earthquake epicenter, in accordance to our previous investigations (Contadakis et al. 2015; Scordilis et al. 2020). We conclude that the LAIC mechanism through acoustic or gravity waves could explain this phenomenology.

References

- Biagi, P.F., Colella, R. Schiavulli, L., Ermini, A., Boudjada, M., Eichelberger, H., Schwingenschuh, K., Katzis, K., Contadakis, M.E., Skeberis, C., Moldovan, I.A. and Bezzeghoud, M. (2019). The INFREP Network: Present Situation and Recent Results. *Open Journal of Earthquake Research*, vol.8, p. 101-115.
- Bruyninx, C., Legrand, J., Fabian, A. and Pottiaux E. (2019). GNSS metadata and data validation in the EUREF Permanent Network, *GPS Solut.* 23: 106. <https://doi.org/10.1007/s10291-019-0880-9>.
- Chatzipetros, A., Pavlides, S., Foumelis, M., Sboras, S., Galanakis, D., Pikridas, C., Bitharis, S., Kremastas, E., Chatziioannou, A., and Papaioannou, I. (2021). The northern Thessaly strong earthquakes of March 3 and 4, 2021, and their neotectonic setting. *Bulletin of the Geological Society of Greece*, 58, 222-255.
- Contadakis, M. E., Arabelos, D.N., Vergos, G., Spatalas, S. D. and Scordilis, E.M., (2015). TEC variations over the Mediterranean before and during the strong earthquake (M=6.5)

- of 12th October 2013 in Crete, Greece, *Physics and Chemistry of the Earth*, 85, 9-16., 2015.
- Dewey, J.F., and A.M.C. Sengör (1979). Aegean and surrounding regions: complex multiplate and continuum tectonics in a convergent zone, *Geol. Soc. Am. Bull.*, 90, 84–92.
- Hayakawa, M. (2011). On the fluctuation spectra of seismo-electromagnetic phenomena, *Nat. Hazards Earth Syst. Sci.*, 11,301-308
- Hayakawa, M., Kasahara, Y., Nakamura, T., Hobara, Y., Rozhnoi, A., Solovieva, M., Molchanov, O.A. and Korepanov, V.(2011). Atmospheric gravity waves as a possible candidate for seismo-ionospheric perturbations, *J. Atmos.Electr.*, 32, 3, 129-140.
- Hayakawa, M., Asano, T., Rozhnoi, A. and Solovieva, M. (2018). Very-low- and low-frequency sounding of ionospheric perturbations and possible association with earthquakes. In *Pre-earthquake Processes: A multidisciplinary approach to earthquake prediction studies*, Ed. by D. Ouzounov et al., 277-304, AGU Book, Wiley.
- Hobara, Y., Lefeuvre, F., Parrot, M., and Molchanov, O.A. (2005). Low-latitude ionospheric turbulence observed by Aureol-3 satellite, *Annales Geophysicae*, 23, 1259–1270.
- Horie, T., Maekawa, S., Yamauchi, T. and Hayakawa, M. (2007). A possible effect of ionospheric perturbations associated with the Sumatra earthquake, as revealed from subionospheric very-low-frequency (VLF) propagation (NWC-Japan), *International Journal of Remote Sensing*, 28, 13, 3133-3139./
- Karakostas, V., Papazachos, C., Papadimitriou, E., Fomelis, M., Kiratzi, A., Pikridas, C., Kostoglou, A., Kkallas, C., Chatzis, N., Bitharis, S., Chatzipetros, A., Fotiou, A., Ventouzi, C., Karagianni, E., Bonatis, P., Kourouklas, C., Paradisopoulou, P., Scordilis, E., Vamvakaris, D., Grendas, I., Kementzetzidou, D., Panou, A., Karakaisis, G., Karagianni, I., Hatzidimitriou, P. and Galanis, O. (2021). The March 2021 Tirnavos, central Greece, doublet (Mw6. 3 and Mw6. 0): Aftershock relocation, faulting details, coseismic slip and deformation. *Bulletin of the Geological Society of Greece*, 58, 131-178.
- Kruse, S. and Royden, L.H. (1994). Bending and unbending of an elastic lithosphere: the Cenozoic history of the Apennine and Dinaride fore deep basins. *Tectonics*, 13, 278-302.
- LePichon X. and J. Angelier (1979). The Hellenic arc and trench system: a key to the neotectonic evolution of the eastern Mediterranean area, *Tectonophysics*, 60, 1-42.
- LePichon X. and J. Angelier (1981). The Aegean Sea, *Philos. Trans. Royal Soc. London*, A300, 357-372.
- McKenzie D.P. (1972). Active tectonics of the Mediterranean region. *Geophys. J. R. Astr. Soc.*, 30, 109-185.
- McKenzie D.P. (1978). Active tectonics of the Alpine-Himalayan belt: the Aegean Sea and surrounding regions, *Geophys. J. R. Astr. Soc.*, 55, 217-254.
- Miyaki, K., Hayakawa, M. and Molchanov, O.A. (2002). The role of gravity waves in the lithosphere-atmosphere-ionosphere coupling, as revealed from the sub-ionospheric LF. propagation, in *Seismo Electromagnetics: Lithosphere-Atmosphere-Ionosphere Coupling*, Ed. by M. Hayakawa and O.A. Molchanov, TERRAPUB, Tokyo, 229-232.
- Molchanov, O., Biagi, P.F., Hayakawa, M., Lutikov, A., Yunga, S., Iudin, D., Andreevsky, S., Rozhnoi, A., Surkov, V., Chebrov, V., Gordeev, E., Schekotov, A. and Fedorov, E.

- (2004). Lithosphere-atmosphere-ionosphere coupling as governing mechanism for preseismic short-term events in atmosphere and ionosphere, *Nat. Hazards Earth Syst. Sci.*, 4, 5/6, 757-767.
- Molchanov, O., Schekotov, A., Solovieva, M., Fedorov, E., Gladyshev, V., Gordeev, E., Chebrov, V., Saltykov, D., Sinitsin, V.I., Hattori, K. and Hayakawa, M. (2005). Near seismic effects in ULF fields and seismo-acoustic emission: statistics and explanation, *Nat. Hazards Earth Syst. Sci.*, 5, 1-10.
- Oral, M.B., Reilinger, R.E., Toksoz, M.N., King R.W., Barka A.A., Kiniki, J and D. Lenk (1995). Global Positioning System offers evidence of plate motions in Eastern Mediterranean, *EOS*, 76, 9-11.
- Papazachos B.C. and P.E. Comninakis, (1970). Geophysical features of the Greek Island Arc and Eastern Mediterranean Ridge. *Com. Ren. Des Seances de la Conference Reunie a Madrid, 1969*, 16, 74-75.
- Papazachos B.C. and P.E. Comninakis (1971). Geophysical and tectonic features of the Aegean arc. *J. Geophys. Res.*, 76, 8517-8533.
- Papazachos, B.C., E.E. Papadimitriou, A.A. Kiratzi, C.B. Papazachos and E.K. Louvari (1998). Fault plane solutions in the Aegean and the surrounding area and their tectonic implications, *Boll. Geof. Teor. Appl.*, 39, 199–218.
- Papazachos, C.B. (1999). Seismological and GPS evidence for the Aegean-Anatolia interaction. *Geophys. Int. Lett.*, 26, 2653-2656.
- Pikridas, C., Bitharis, S., Katsougiannopoulos, S., Spanakaki, K. and Karolos, I.A. (2019). Study of TEC variations using permanent stations GNSS data in relation with seismic events. Application on Samothrace earthquake of 24 May 2014. *Geodesy and cartography*, 45(3), 137-146.
- Ritsema, A.R. (1974). The earthquake mechanism in Balkan region. *Inst. Sci. Rep.*, 74, 1-36.
- Schaer, S., Gurtner, W. and Feltens, J. (1998). IONEX: The ionosphere map exchange format version 1. *Proceedings of the IGS AC workshop*, Darmstadt, Germany. Vol. 9. No. 11.
- Scordilis E.M., Contadakis M.E, Vallianatos F. and Spatalas S. (2020). Lower Ionospheric turbulence variations during the intense tectonic activity in Eastern Aegean area, *Annals of Geophysics*, 63, 5, PA544.
- Seemala, G.K. and Valladares, C.E. (2011). Statistics of total electron content depletions observed over the South American continent for the year 2008, *Radio Science*, 46, RS5019, doi:10.1029/2011RS004722.
- Turcotte D.L. (1997). *Fractal and Chaos in Geology and Geophysics* (2nd Edition), Cambridge University Press, Cambridge U.K.